Journal of Materials Chemistry A

Accepted Manuscript

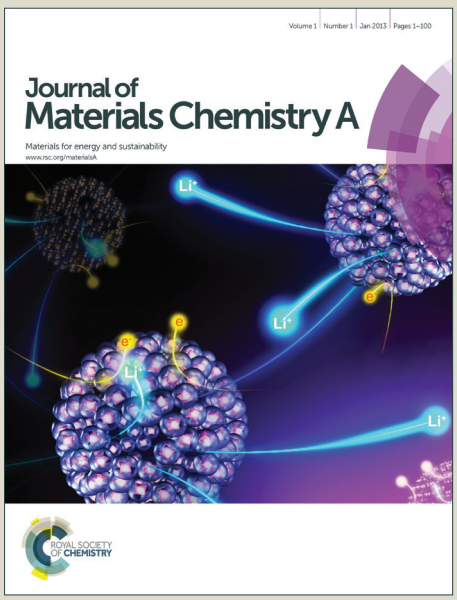

ROYAL SOCIETY OF CHEMISTRY

www.rsc.org/materialsA

Thermoelectric properties of Ge doped n-type $Ti_xZr_{1-x}NiSn_{0.975}Ge_{0.025}$ half-Heusler alloys

Yuanfeng Liu[1], Pierre F.P. Poudeu[1, *]

1) Laboratory for Emerging Energy and Electronic Materials, Department of Materials Science and Engineering, University of Michigan, Ann Arbor, 48109, USA

*Corresponding author. Tel: +1-734-763-8436; Fax: +1-734-763-4788

Email: ppoudeup@umich.edu (PFPP)

Keywords: Keywords: Thermal conductivity · Nanostructures · Germanium-doped Semiconductor · Half-Heusler · Thermoelectrics

RECEIVED DATE …….

Abstract

Several compositions of the *n-type*, $Ti_xZr_{1-x}NiSn_{0.975}Ge_{0.025}$ (x = 0, 0.1, 0.15 and 0.25), half-Heusler (HH) alloys were synthesized by reacting elemental powders at high temperature using induction melting. The resulting ingots were annealed at 900 °C for 2 weeks and mechanically alloyed to achieve fine grain size. X-ray powder diffraction suggested the formation of products with HH structure. However, electron microscopy studies revealed phase separation into Ti-rich and Zr-rich domains for the ingot with x = 0.25. The effect of band gap engineering through isoelectronic substitution of Sn by Ge and mass fluctuation arising from the intermixing of Ti and Zr in the HH structure on the electronic and thermal transports in the temperature range from 300 K to 775 K was investigated. A large reduction in the lattice thermal conductivity (4.9 W/Km to 2.8 W/Km at 300 K) was observed with increasing Ti concentration. Surprisingly, the thermopower and electrical conductivity for the sample with x = 0.25 simultaneously increase with rising temperature from -120 μV/K and 510 S/cm at 300 K to -160 μV/K and 840 S/cm at 775 K. The combination of large reduction in lattice thermal conductivity via mass fluctuation at the Ti/Zr site with optimization of the thermopower and electrical conductivity through Ge substitution at the Sn site significantly improved the figure of merit from 0.05 to 0.48 at 775 K for the sample with x = 0.25.

Introduction

As energy demands are increasing, alternative renewable energy sources such as thermoelectric devices, which can directly convert heat to electrical energy, are attracting more attention. The performance of a thermoelectric material is characterized using the thermoelectric figure of merit, $ZT = \sigma S^2 T/\kappa$, where σ is the electrical conductivity, S is the thermopower, T is the absolute temperature and κ is the thermal conductivity [1-2]. The efficiency of a thermoelectric device depends on the temperature range over which the material exhibits sufficiently large ZT values. For instance, SiGe-based materials are suitable for applications in the temperature range from 700K to ~1200 K [3-4], while PbTe-based materials operate under moderate temperatures (500 K ~ 800K) [5-6].

Half-Heusler (HH) alloys are promising thermoelectric materials for applications in the temperature range from 700 K to 900 K, which is comparable to the temperature of industrial waste heat [7-9]. HH alloys are intermetallic compounds crystallizing with MgAgAs structure, which consists of four interpenetrating *fcc* (face centered cubic) sublattices.[10] Most studied HH alloys are based on *n-type* MNiSn [11-13] and *p-type* MCoSb [14-16], where M = Ti, Zr, Hf or the intermixing of these elements. Because the constituting elements are environmentally friendly and cheap, these families of HH alloys can be used in large-scale applications such as on vehicle exhaust systems and industrial power plants [17-19]. HH alloys with 18 valence electrons have narrow band gaps, leading to a relatively high Seebeck coefficient and electrical conductivity. However, their thermal conductivity can reach ~ 10 $WK^{-1}m^{-1}$ at the room temperature resulting in low ZT values [13, 20-22]. The main strategy for increasing the *ZT* value of HH alloys consists of reducing thermal conductivity through enhanced phonon scattering. This can be achieved by increasing mass fluctuation or point defects in the sample [23-27]. Alternatively, thermal conductivity of HH alloys is reduced using second phases as additional phonon scattering centers in the samples [28-29]. In our previous research, we focused on coherently embedding full-Heusler (FH) phases as nanostructures in bulk HH alloys [23-25, 29-31]. The FH phase, which is structurally related to the HH matrix, was formed by adding excess Ni in the starting mixture, resulting in the formation of a bulk HH/FH composite via solid-state reaction [23, 30-31]. The resulting bulk HH composite with nanostructured FH particles exhibited improved electronic properties and low thermal conductivity arising from enhanced phonon scattering at multiple HH/FH coherent interfaces. For example, the lattice thermal conductivity of $Ti_{0.1}Zr_{0.9}Ni_{1+x}Sn$ nanocomposites

could be reduced to 4.75 $WK^{-1}m^{-1}$ at 775 K [23]. Furthermore, we observed that the addition of a small amount of Sb at Sn sites in $Ti_{0.1}Zr_{0.9}Ni_{1+x}Sn$ nanocomposites resulted in a constant Seebeck coefficient and electrical conductivity, while the lattice thermal conductivity was effectively reduced to ~ 4.4 $WK^{-1}m^{-1}$ at 775 K [30].

Most studies in *n-type* MNiSn HH systems are focused on the intermixing of two or three elements at the M site, or the substitution of Sn by a small amount of a heavier element, such as Sb or Bi, to enhance phonon scattering [32-37]. However, studies exploring mass fluctuation at both M and Sn positions in MNiSn HH alloys are scarce. In this work, we explore the effect of band gap engineering through isoelectronic substitution of Sn by Ge and mass fluctuation arising from the intermixing of Ti and Zr on the thermoelectric properties of $Ti_xZr_{1-x}NiSn_{0.975}Ge_{0.025}$ (x = 0, 0.1, 0.15 and 0.25) composites synthesized by induction melting of the elements followed by mechanical alloying using high energy shaker ball milling. All samples were consolidated under the same condition using a uniaxial hot pressing system. Scanning electron microscopy (SEM) and high-resolution transmission electron microscopy (HRTEM) revealed the presence of Ti-rich and Zr-rich phases in bulk ingots obtained from composition with x = 0.25. We found that the substitution of 2.5% Sn by Ge in $Ti_{0.1}Zr_{0.9}NiSn_{0.975}Ge_{0.025}$ led to large reduction in the thermal conductivity and marginal change in the electrical conductivity and thermopower. This markedly differs from the effect of Sb-doping at Sn sites ($Ti_{0.1}Zr_{0.9}NiSn_{0.975}Sb_{0.025}$), where significant increase in the electrical conductivity and large reduction in the thermopower was observed.[30] In addition, we found that increasing Ti concentration in $Ti_xZr_{1-x}NiSn_{0.975}Ge_{0.025}$ resulted in a simultaneous increase in the thermopower and additional reduction in the thermal conductivity. This large reduction in the thermal conductivity of $Ti_xZr_{1-x}NiSn_{0.975}Ge_{0.025}$ is attributed to the introduction of mass fluctuation at both M and Sn sites in MNiSn HH alloys.

Experimental

Synthesis. Ingots of $Ti_xZr_{1-x}NiSn_{0.975}Ge_{0.025}$ were first prepared by melting a mixture of high purity elements (Ti, Zr, Ni, Sn and Sb > 99.9%) in the desired stoichiometry using an induction furnace. In order to prevent oxidation during induction melting, the sample mixture was first sealed in a quartz tube under a residual pressure of 10^{-3} Torr. In addition, the induction melting chamber was maintained under the vacuum during the synthesis. Each ingot was melted three times to ensure homogeneity. The resulting ingots were thoroughly ground under argon

atmosphere using an agate mortar and pestle. The polycrystalline powder was sealed in a quartz tube under a residual pressure of 10^{-3} Torr and annealed sequentially to 300 °C for 3 days then to 900 °C for 7 days. The annealed powder was then loaded into a stainless-steel jar with stainless-steel balls for a 2 hr mechanical alloying process using a SPEX Sample Prep Mixer/Mill. The resulting powder was consolidated into a pellet at 950 °C under 100 MPa using a uniaxial hot press. The relative density of $Ti_xZr_{1-x}NiSn_{0.975}Ge_{0.025}$ pellets used for in this study was above 95%.

Characterization. The structure and phase purity of the as-prepared powder with different Ti/Zr ratios was examined by powder X-ray diffraction (PXRD) using monochromated Cu-Kα radiation on a rotating anode Rigaku diffractometer operating at 40 kV and 100 mA. The internal structure of hot pressed pellets was examined by a scanning electron microscope (SEM, Philips XL30FEG) and a high-resolution transmission electron microscope (HRTEM, JEOL 3011). The thermopower and electrical conductivity were measured simultaneously from room temperature to 500 °C under a low pressure He atmosphere using a commercial ZEM-3 system from ULVAC-RIKO. The instrument precision on thermopower and electrical conductivity data is ± 4%. The thermal conductivity was calculated from thermal diffusivity data measured by the laser flash method (Linseis, LFA 1000) from room temperature to 500 °C under dynamic vacuum (~10^{-3} Torr). The instrument precision on thermal diffusion data is ± 5%.

Results and discussion

Phase stability. Figure 1A shows the X-ray powder diffraction patterns of the synthesized $Ti_xZr_{1-x}NiSn_{0.975}Ge_{0.025}$ (x = 0, 0.1, 0.15 and 0.25) samples after heat treatment and after the mechanical alloying steps. All peaks from the XRD patterns can be indexed with the MgAgAs structure type suggesting the formation of HH alloys. A careful examination of XRD patterns of $Ti_xZr_{1-x}NiSn_{0.975}Ge_{0.025}$ (x = 0, 0.1, 0.15 and 0.25) reveals a shift of the (2 2 0) peak towards higher angles when Ti concentration increases. This indicates the substitution of large Zr (155 ppm) atoms by smaller Ti (140 ppm) atoms in the ZrNiSn structure. This result is consistent with previous studies [36, 38-39]. Figure 1B shows the change in the lattice parameter of all samples, after heat treatment, with increasing Ti concentration. The calculated lattice parameters slightly deviate from Vegard's law, which suggests the formation of multiple phases. This analysis is

supported by the broadening of the (2 2 0) peak with increasing Ti concentration, which also indicates intrinsic phase separation into Ti-rich and Zr-rich phases (Figure 1A).

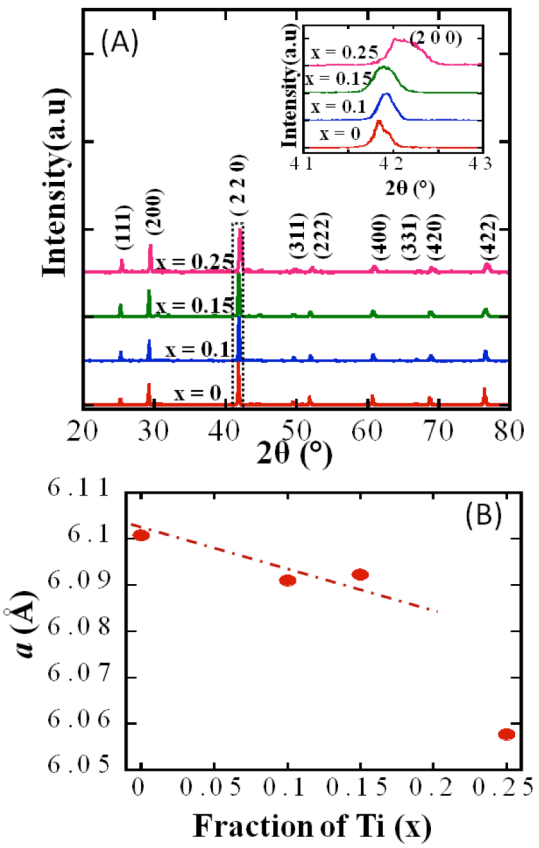

Figure 1: (A) X-ray diffraction pattern of $Ti_xZr_{1-x}NiSn_{0.975}Ge_{0.025}$ (x = 0, 0.1, 0.15 and 0.25) samples after heat treatment and mechanical alloying. The insert shows the broadening of the (220) peak with increasing Ti concentration, indicating intrinsic phase separation into Ti-rich and Zr-rich phases; (B) Lattice parameters calculated from the XRD patterns of $Ti_xZr_{1-x}NiSn_{0.975}Ge_{0.025}$ (x = 0, 0.1, 0.15 and 0.25) samples after heat treatment.

Figure 2A shows a back-scattered electron (BSE) SEM image of a specimen cut from a pressed pellet with nominal composition $Ti_{0.25}Zr_{0.75}NiSn_{0.975}Ge_{0.025}$ indicating the presence of two distinct phases within the bulk material. The light gray area is attributed to Zr-rich (heavy element) HH phase, whereas the dark gray area is believed to be Ti-rich (lighter element) HH phase. This result is also consistent with the broadening of (2 2 0) peaks, which suggests the coexistence of two HH phases with similar lattice parameters (Ti-rich and Zr-rich HH phases). It is interesting to note the formation, for the sample with x = 0.25, of nanometer-scale phases within the matrix (Figure 2C), in contrary to previous studies.[40-41] The formation of such fine nanometer scale features results from the mechanical alloying steps following the formation of $Ti_xZr_{1-x}NiSn_{0.975}Ge_{0.025}$ samples through induction melting of elemental powders. As can be observed from the low magnification TEM imaging (Figure 2B), these features appear as dark particles dispersed in a bright matrix. These nanoscale dark spots are believed to be Ti-rich particles, which are separated in the nanometer range by Zr-rich regions. Some of the Ti-rich nanostructures overlap to form large agglomerates. From Figure 2C, it can be seen that particles of a Ti-rich phase is formed by agglomeration of small crystals with different orientations. The lattice parameter, a = 6.12 Å,

calculated from the SAED pattern (Figure 2D) is comparable to the lattice parameter of $ZrNiSn_{0.975}Ge_{0.025}$ further confirming that the matrix is Zr-rich.

Thermoelectric properties. In our earlier work,[23] [30] we demonstrated that the substitution of a small amount (2.5%) of Sb at Sn site in the structure of $Ti_{0.1}Zr_{0.9}NiSn$ [23] led to the heavily doped $Ti_{0.1}Zr_{0.9}NiSn_{0.975}Sb_{0.025}$ semiconductor with a slight improvement of the thermoelectric properties. [30] In the current work, we assess the effect of band gap engineering through isoelectronic substitution of 2.5% Ge at Sn site on the thermoelectric behavior of $Ti_{0.1}Zr_{0.9}NiSn_{0.975}Ge_{0.025}$ system. Figure 3 shows a comparison of the temperature dependent thermoelectric properties of the $Ti_{0.1}Zr_{0.9}NiSn_{0.975}Ge_{0.025}$ samples with data previously reported for the $Ti_{0.1}Zr_{0.9}NiSn$[23] and $Ti_{0.1}Zr_{0.9}NiSn_{0.975}Sb_{0.025}$[30]samples synthesized by solid-state reactions of the elements. Regardless of the temperature, the highest electrical conductivity is observed for the Sb-doped sample, $Ti_{0.1}Zr_{0.9}NiSn_{0.975}Sb_{0.025}$. This is consistent with the expected increase in the carrier density upon substituting Sn by Sb in the structure of $Ti_{0.1}Zr_{0.9}NiSn$. The electrical conductivity of the $Ti_{0.1}Zr_{0.9}NiSn_{0.975}Sb_{0.025}$ sample decreases with increasing temperature, which is consistent with heavily doped semiconducting behavior.

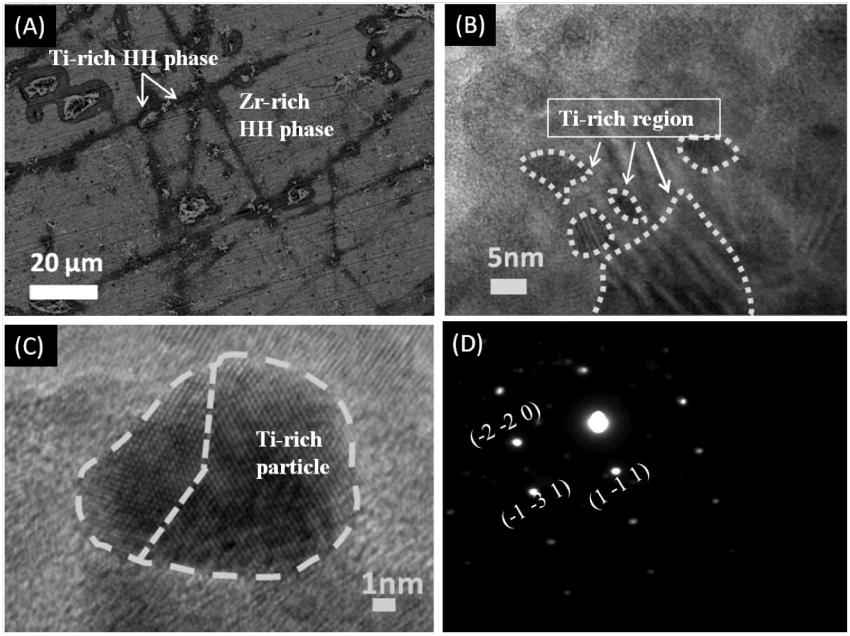

Figure 2: Electron microscopy study of $Ti_{0.25}Zr_{0.75}NiSn_{0.975}Ge_{0.025}$ (x = 0, 0.1, 0.15 and 0.25) composites. (A) Back scattering electron (BSE) of SEM image, showing micron size Ti-rich phase in Zr-rich matrix; (B) low magnification TEM image, showing 10 nm Ti-rich phase embedded inside Zr-rich matrix; (C) high magnification TEM image, showing the crystallization of the Ti-rich nanophase ; (D) selected area electron diffraction (SAED) pattern, indicating the *fcc* structure of Zr-rich HH matrix.

Interestingly, the electrical conductivity of $Ti_{0.1}Zr_{0.9}NiSn_{0.975}Ge_{0.025}$ is higher than that of $Ti_{0.1}Zr_{0.9}NiSn$ at temperatures above 300 K. This is a quite surprising result. While the isoelectronic substitution of Ge at Sn sites in the structure of $Ti_{0.1}Zr_{0.9}NiSn$ is not expected to contribute additional carriers (i.e. constant carrier density) to the conduction band, a slight increase in the electrical band gap can be anticipated. This should result in a drop in the carrier density, at a given temperature, when compared to undoped $Ti_{0.1}Zr_{0.9}NiSn$ matrix. Therefore, lower electrical conductivity and higher thermopower would be expected for $Ti_{0.1}Zr_{0.9}NiSn_{0.975}Ge_{0.025}$ compared to $Ti_{0.1}Zr_{0.9}NiSn$ system. However, the observed higher electrical conductivity and lower thermopower for $Ti_{0.1}Zr_{0.9}NiSn_{0.975}Ge_{0.025}$ imply a reduction in the electrical band gap $Ti_{0.1}Zr_{0.9}NiSn$ upon isoelectronic substitution of Sn by Ge. One possible explanation of the reduction of the electrical band gap is that the substitution of Sn by Ge instead of modifying the band structure of the matrix creates impurity states within the band gap. This results in lower activation energy and an increase in the concentration of thermally excited carriers at a given temperature. This is consistent with the lower thermopower values observed at high temperatures for Ge-substituted samples. The electrical conductivity of $Ti_{0.1}Zr_{0.9}NiSn$ and $Ti_{0.1}Zr_{0.9}NiSn_{0.975}Ge_{0.025}$ increases with rising temperature, indicating intrinsic semiconducting behavior.

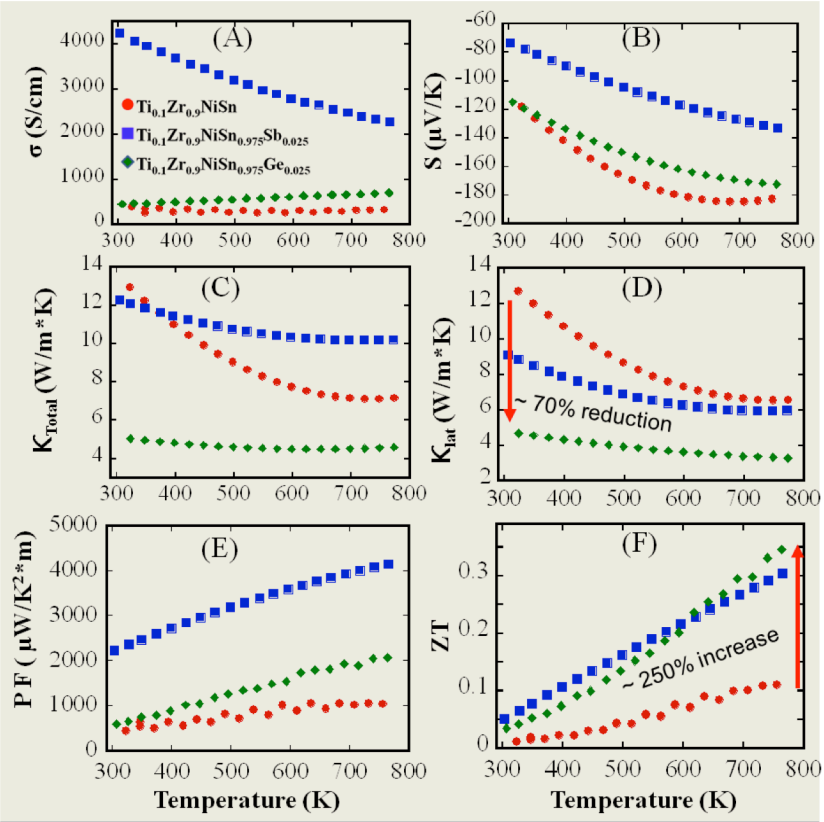

Figure 3: Temperature dependence of (A) electrical conductivity; (B) thermopower; (C) thermal conductivity; (D) lattice thermal conductivity; (E) power factor and (F) figure of merit of $Ti_{0.1}Zr_{0.9}NiSn$; $Ti_{0.1}Zr_{0.9}NiSn_{0.975}Sb_{0.025}$ and $Ti_{0.1}Zr_{0.9}NiSn_{0.975}Ge_{0.025}$ samples.

Figure 3C and 3D show the temperature dependence of total thermal conductivity and lattice thermal conductivity of $Ti_{0.1}Zr_{0.9}NiSn$, $Ti_{0.1}Zr_{0.9}NiSn_{0.975}Sb_{0.025}$ and $Ti_{0.1}Zr_{0.9}NiSn_{0.975}Ge_{0.025}$ samples. The thermal conductivity of all samples decreases with increasing temperature. Regardless of the temperature, the Ge-substituted sample exhibits the lowest total thermal conductivity. At 300 K, the total thermal conductivity decreases from 13 $Wm^{-1}K^{-1}$ for the undoped sample to 5 $Wm^{-1}K^{-1}$ upon substitution of Sn by 2.5 % Ge. The lattice thermal conductivity (κ_L) was obtained by subtracting electronic thermal conductivity (κ_e) from total thermal conductivity, κ. κ_e was estimated through Wiedemann-Franz law, $\kappa_e = L_o \sigma T$, where $L_o = 2.45 \times 10^{-8}$ $W\Omega K^{-2}$ is Lorenz number. The lattice thermal conductivity of all samples also follows similar trend with the total thermal conductivity. At 300 K, the lattice thermal conductivity of $Ti_{0.1}Zr_{0.9}NiSn$ is 12.6 $Wm^{-1}K^{-1}$. Upon substituting of 2.5% Sn by Sb, the lattice thermal conductivity of $Ti_{0.1}Zr_{0.9}NiSn_{0.975}Sb_{0.025}$ decreases to 9 $Wm^{-1}K^{-1}$. Interestingly, the substitution of Sn by 2.5 % Ge in $Ti_{0.1}Zr_{0.9}NiSn$ results in a remarkable reduction in the lattice thermal conductivity to ~5 $Wm^{-1}K^{-1}$ at 300 K. At 775 K, $Ti_{0.1}Zr_{0.9}NiSn$ and $Ti_{0.1}Zr_{0.9}NiSn_{0.975}Sb_{0.025}$ have similar values of the lattice thermal conductivity (~ 6 $Wm^{-1}K^{-1}$), whereas the lattice thermal conductivity of $Ti_{0.1}Zr_{0.9}NiSn_{0.975}Ge_{0.025}$ reaches 2.7 $Wm^{-1}K^{-1}$. The low total thermal conductivity of $Ti_{0.1}Zr_{0.9}NiSn_{0.975}Ge_{0.025}$ is attributed to high phonon scattering arising from the combination of (1) mass fluctuation due to Ge/Sn substitution and (2) high-density grain boundaries from particle size refinement by mechanical alloying. This large difference in the thermal conductivity of $Ti_{0.1}Zr_{0.9}NiSn_{0.975}Ge_{0.025}$ and $Ti_{0.1}Zr_{0.9}NiSn$ samples results from the grain size refinement of the synthesized $Ti_{0.1}Zr_{0.9}NiSn_{0.975}Ge_{0.025}$ powders by mechanical alloying.

The temperature dependence of the power factor calculated using the electrical conductivity and thermopower data for $Ti_{0.1}Zr_{0.9}NiSn$; $Ti_{0.1}Zr_{0.9}NiSn_{0.975}Sb_{0.025}$ and $Ti_{0.1}Zr_{0.9}NiSn_{0.975}Ge_{0.025}$ is shown in Figure 3E. It can be seen that the substitution of Sn by 2.5 % Sb leads to a drastic increase in the power factor, which is mostly due to the large increase in the carrier concentration. However, the substitution of Sn by Ge is isoelectronic; therefore, the increase in the power factor on the Ge-substituted sample cannot be explained only by considering the increase in the carrier concentration arising from the reduction in the band gap as discussed above. This is due to the fact that an increase in the electrical conductivity through thermal excitation of electrons from the valence band (or impurity band) to the conduction band

would normally be offset by a reduction in the thermopower. Therefore, the observed enhancement of the power factor of Ge-substituted sample compared to the undoped Sn sample suggests that the observed increase in the electrical conductivity is not completely offset by a reduction in the thermopower. This can be explained by considering an enhancement in the overall carrier mobility for Ge-substituted sample. The *ZT* value at 775 K for the Ge-substituted sample is slightly larger than that of Sb-doped sample. This is due to the combination of drastic reduction in the thermal conductivity and marginal increase in the power factor which leads to a 250 % increase in the figure of merit (0.35 at 775 K) compared to undoped sample.

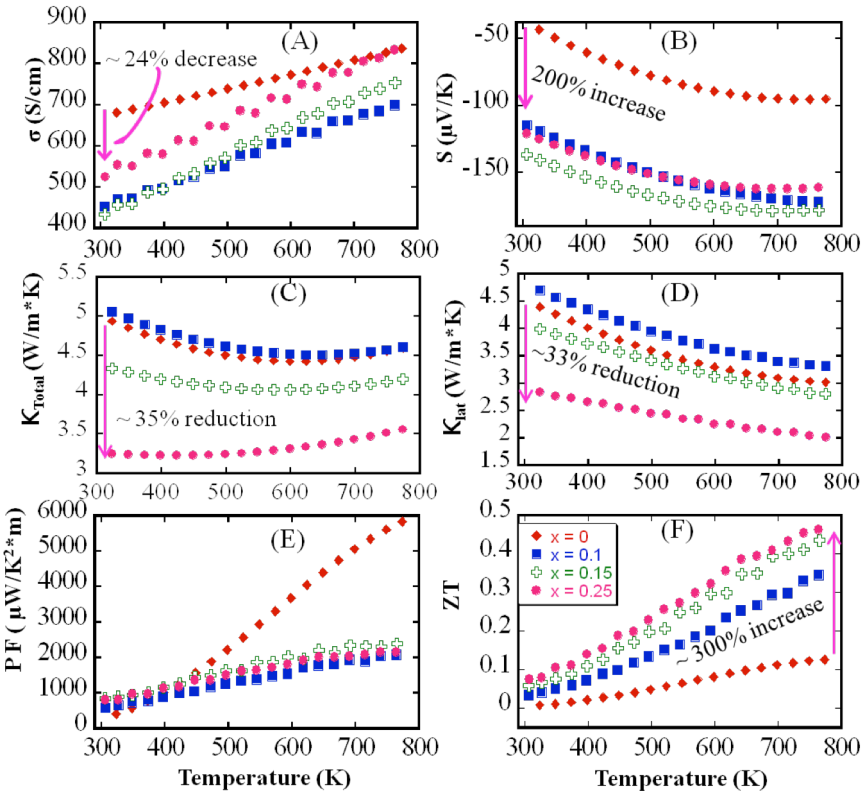

Figure 4: Temperature dependence of (A) electrical conductivity; (B) thermopower; (C) thermal conductivity; (D) lattice thermal conductivity; (E) power factor and (F) figure of merit of $Ti_xZr_{1-x}NiSn_{0.975}Ge_{0.025}$ (x = 0, 0.1, 0.15 and 0.25) samples.

In order to probe the effect of the Ti/Zr ratio on the thermoelectric properties of $Ti_xZr_{1-x}NiSn_{0.975}Ge_{0.025}$ alloys, various compositions with x = 0, 0.1, 0.15 and 0.25 were synthesized and their thermoelectric properties were measured from 300 K to 775 K (Figure 4). The electrical conductivity of all these samples increased with rising temperature indicating intrinsic semiconducting behavior. Regardless of the temperature, the largest electrical conductivity is observed for the sample with x = 0 ($ZrNiSn_{0.975}Ge_{0.025}$). At 300 K, the electrical conductivity initially decreases from 680 S/cm for the sample with x = 0 to 440 S/cm for the sample with x = 0.1 and 0.15 then slightly increase to 520 S/cm for the sample with x = 0.25 (Figure 4A).

To better understand the reason behind the change of the electrical conductivity, the band gap (E_g) was calculated by fitting the conductivity curve, in the temperature range from 300 K to 775 K, using the Arrhenius equation, $\sigma = \sigma_0 exp^{-\frac{E_g}{2kT}}$. It was found that the band gap increases with increasing Ti concentration (Figure 5), reaching the highest value (E_g = 81meV) for the sample with x = 0.15 and decreasing to 41 meV with further increase in Ti concentration to x = 0.25. Therefore, the observed decrease in the electrical conductivity upon increasing the Ti content from 0 to 0.15 can be associated with the drop in the carrier concentration at a given temperature due to an increase in the band gap. Interestingly, this trend is broken for the sample with x = 0.25, in which an increase in the carrier concentration (smaller band gap) is observed. This deviation from the general trend can be associated to the phase separation into Zr-rich matrix with Ti-rich nanostructures observed in the sample with x = 0.25 (Figure 2), instead of the solid-solutions observed for samples with x ≤ 0.15. In such composites, both the Zr-rich phase with high electrical conductivity and the Ti-rich phase with poor electrical conductivity contribute to the observed overall electrical conductivity of the sample. The electrical conductivity of the sample with x = 0.25 rapidly increases with rising temperature reaching a value similar to that of $ZrNiSn_{0.975}Ge_{0.025}$ at 775 K.

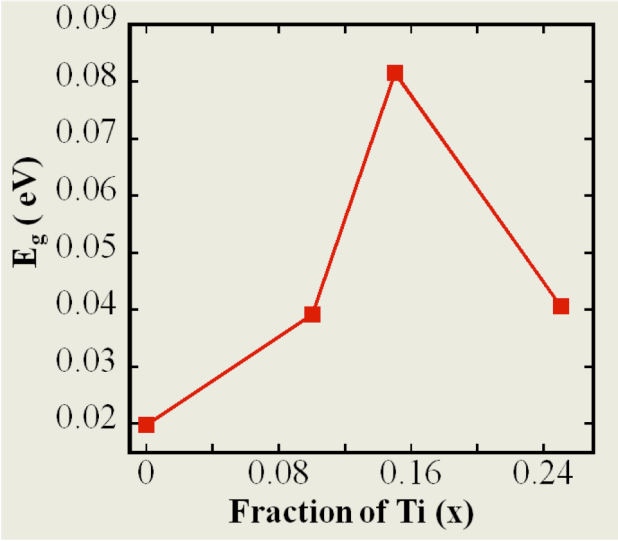

Figure 5: Band gap calculated from the electrical conductivity of $Ti_xZr_{1-x}NiSn_{0.975}Ge_{0.025}$ (x = 0, 0.1, 0.15 and 0.25) samples.

Figure 4B shows the temperature dependence of the thermopower of $Ti_xZr_{1-x}NiSn_{0.975}Ge_{0.025}$ samples. All samples show negative thermopower indicating *n-type* semiconducting behavior. At 300 K, the thermopower increases with Ti concentration from -40 μV/K for the sample with x = 0 to -140 μV/K for the sample with x = 0.15, then decreases to -120 μV/K upon increasing the Ti concentration to x = 0.25. Regardless of the composition, the absolute themopower increases with increasing temperature. At 775 K, the largest thermopower value of -180 μV/K is observed for the sample with x = 0.15. The most surprising result here is

the large difference in the thermopower values of samples with x = 0 and 0.25 at 775 K, despite the similarity in their electrical conductivity. To rationalize this result, one must take into account the role of Ti-rich nanostructures on the electronic transport within the Zr-rich matrix. As demonstrated above, the substitution of 25% Zr by Ti results in a phase separation into microscale and nanometer-scale Ti-rich inclusions within the Zr-rich half-Heusler matrix. At 300K, we observed a small reduction (~24%) in the electrical conductivity (from 680 S/cm for x = 0 to 520 S/cm for x = 0.25) and drastic increase (~200%) in the thermopower (from -40 μV/K for x = 0 to -120 μV/K for x = 0.25) of the sample with x = 0.25 when compared to the pure matrix.

The total thermal conductivity and lattice thermal conductivity of $Ti_xZr_{1-x}NiSn_{0.975}Ge_{0.025}$ samples are plotted in Figure 4C and 4D. The total thermal conductivity at a given temperature decreases with increasing Ti concentration. At 300 K, the total thermal conductivity decreases from ~ 5 $Wm^{-1}K^{-1}$ for x = 0 to ~3.25 $Wm^{-1}K^{-1}$ for x = 0.25. Regardless of the composition, the total thermal conductivity initially decreases with rising temperature to reach a minimum then increases with further increase in temperature. This trend can be ascribed to the effect of bipolar conduction at temperatures above the temperature of minimum thermal conductivity. The lattice thermal conductivity of the $Ti_xZr_{1-x}NiSn_{0.975}Ge_{0.025}$ samples decrease with increasing temperature (Figure 4D). The lowest lattice thermal conductivity (2 $Wm^{-1}K^{-1}$ at 775 K) is observed for the sample with x = 0.25. The observed large reduction in the lattice thermal conductivity with increasing Ti concentration can be explained by (1) mass fluctuation phonon scattering due to intermixing of Ti/Zr at the same atomic site and (2) enhanced phonon scattering at the nanometer scale and micrometer scale phase boundary between the Zr-rich HH matrix and Ti-rich HH inclusions and grain boundaries in $Ti_{0.25}Zr_{0.75}NiSn_{0.975}Ge_{0.025}$ composite.

Figure 4E displays the temperature dependence of the power factor of all $Ti_xZr_{1-x}NiSn_{0.975}Ge_{0.025}$ samples. At 300 K, all samples show a similar power factor of ~ 900 $\mu W/K^2m$. As the temperature increases, the power factor of the sample with x = 0 rapidly increases to ~ 6000 $\mu W/K^2m$ at 775 K. However, the samples with x = 0.1, 0.15 and 0.25 show much lower power factor (~ 2100 $\mu W/K^2m$) at 775 K. Despite the relatively low power factor of Ti containing samples, the observed low thermal conductivity results in large enhancements of the figure of merit when compared to the sample with x = 0 (Figure 4F). At 300 K, *ZT* values

increase with Ti concentration from 0.05 to 0.08. As the temperature increases, the *ZT* values of various samples increase, reaching a maximum of 0.48 at 775 K for the sample with x = 0.25.

Conclusion

In summary, we have examined the effects of Ge substitution at Sn sites and of Ti substitution at Zr sites (varying Ti/Zr ratios) on the thermoelectric properties of $Ti_xZr_{1-x}NiSn_{0.975}Ge_{0.025}$ (x = 0, 0.1, 0.15 and 0.25) series of samples produced by induction melting and mechanical alloying. We found that increasing the Ti concentration above x = 0.15 led to a phase separation in the bulk $Ti_xZr_{1-x}NiSn_{0.975}Ge_{0.025}$ samples with the formation of Ti-rich inclusions embedded into the Zr-rich matrix. This combination of partial solid solution and phase separation in $Ti_xZr_{1-x}NiSn_{0.975}Ge_{0.025}$ resulted in a large reduction in the thermal conductivity. In addition, we observed an increase in the thermopower with increasing Ti concentration leading to an improvement in the power factor when compared to the sample with x = 0. The simultaneous increase in the power factor and large reduction in the thermal conductivity of $Ti_xZr_{1-x}NiSn_{0.975}Ge_{0.025}$ samples resulted in a large increase in the *ZT* with a maximum value of 0.48 observed at 775 K for $Ti_{0.25}Zr_{0.75}NiSn_{0.975}Ge_{0.025}$ composites. This work demonstrates that by manipulating the band gap of half-Heusler alloys through isoelectronic substitution at Ti/Zr and Sn/Ge sites, simultaneous enhancement of thermopower and reduction in thermal conductivity can be achieved leading to a significant increase in the *ZT* value.

Acknowledgements

We gratefully acknowledge the financial support from the Department of Energy, Office of Basic Energy Science under Award # DE-SC-0008574. This work made use of the TEM from the University of Michigan's Electron Microbeam Analysis Laboratory (EMAL), purchased with funds from the National Science Foundation Awards DMR-0315633 and DMR-0723032.

Reference

[1] G. J. Snyder, E. S. Toberer,Complex thermoelectric materials, *Nature Materials* 2008, ***7***, 105.

[2] C. J. Vineis, A. Shakouri, A. Majumdar, M. G. Kanatzidis,Nanostructured Thermoelectrics: Big Efficiency Gains from Small Features, *Advanced Materials* 2010, ***22***, 3970.

[3] G. Joshi, H. Lee, Y. C. Lan, X. W. Wang, G. H. Zhu, D. Z. Wang, R. W. Gould, D. C. Cuff, M. Y. Tang, M. S. Dresselhaus, G. Chen, Z. F. Ren,Enhanced Thermoelectric Figure-of-Merit in Nanostructured p-type Silicon Germanium Bulk Alloys, *Nano Letters* 2008, ***8***, 4670.

[4] X. W. Wang, H. Lee, Y. C. Lan, G. H. Zhu, G. Joshi, D. Z. Wang, J. Yang, A. J. Muto, M. Y. Tang, J. Klatsky, S. Song, M. S. Dresselhaus, G. Chen, Z. F. Ren,Enhanced thermoelectric figure of merit in nanostructured n-type silicon germanium bulk alloy, *Applied Physics Letters* 2008, ***93***, 193121.

[5] J. P. Heremans, V. Jovovic, E. S. Toberer, A. Saramat, K. Kurosaki, A. Charoenphakdee, S. Yamanaka, G. J. Snyder,Enhancement of thermoelectric efficiency in PbTe by distortion of the electronic density of states, *Science* 2008, ***321***, 554.

[6] Y. Pei, X. Shi, A. LaLonde, H. Wang, L. Chen, G. J. Snyder,Convergence of electronic bands for high performance bulk thermoelectrics, *Nature* 2011, ***473***, 66.

[7] S. R. Culp, S. J. Poon, N. Hickman, T. M. Tritt, J. Blumm,Effect of substitutions on the thermoelectric figure of merit of half-Heusler phases at 800 degree C, *Applied Physics Letters* 2006, ***88***, 042106.

[8] X. Yan, G. Joshi, W. Liu, Y. Lan, H. Wang, S. Lee, J. Simonson, S. Poon, T. Tritt, G. Chen,Enhanced thermoelectric figure of merit of p-type half-Heuslers, *Nano Letters* 2010, ***11***, 556.

[9] C. Yu, T. J. Zhu, R. Z. Shi, Y. Zhang, X. B. Zhao, J. He,High-performance half-Heusler thermoelectric materials $Hf_{1-x}Zr_xNiSn_{1-y}Sb_y$ prepared by levitation melting and spark plasma sintering, *Acta Materialia* 2009, ***57***, 2757.

[10] W. Jeitschko,Transition Metal Stannides with Mgagas and $MnCu_2Al$-Type Structure, *Metallurgical Transactions* 1970, ***1***, 3159.

[11] S. Katsuyama, R. Matsuo, M. Ito,Thermoelectric properties of half-Heusler alloys $Zr_{1-x}Y_xNiSn_{1-y}Sb_y$, *Journal of Alloys and Compounds* 2007, ***428***, 262.

[12] P. F. Qiu, J. Yang, X. Y. Huang, X. H. Chen, L. D. Chen,Effect of antisite defects on band structure and thermoelectric performance of ZrNiSn half-Heusler alloys, *Applied Physics Letters* 2010, ***96***, 152105.

[13] C. Uher, J. Yang, S. Hu, D. T. Morelli, G. P. Meisner,Transport properties of pure and doped MNiSn (M=Zr, Hf), *Physical Review B* 1999, ***59***, 8615.

[14] P. F. Qiu, X. Y. Huang, X. H. Chen, L. D. Chen,Enhanced thermoelectric performance by the combination of alloying and doping in TiCoSb-based half-Heusler compounds, *Journal of Applied Physics* 2009, ***106***, 103703.

[15] T. Wu, W. Jiang, X. O. Li, Y. F. Zhou, L. D. Chen,Thermoelectric properties of p-type Fe-doped TiCoSb half-Heusler compounds, *Journal of Applied Physics* 2007, ***102***, 103705.

[16] W. J. Xie, Q. Jin, X. F. Tang,The preparation and thermoelectric properties of $Ti_{0.5}Zr_{0.25}Hf_{0.25}Co_{1-x}Ni_xSb$ half-Heusler compounds, *Journal of Applied Physics* 2008, ***103***, 043711.

[17] G. Joshi, X. Yan, H. Wang, W. Liu, G. Chen, Z. Ren,Enhancement in Thermoelectric Figure Of Merit of an n-Type Half-Heusler Compound by the Nanocomposite Approach, *Advanced Energy Materials* 2011, ***1***, 643.

[18] W. Liu, X. Yan, G. Chen, Z. Ren,Recent advances in thermoelectric nanocomposites, *Nano Energy* 2012, ***1***, 42.

[19] M. Schwall, B. Balke,Niobium substitution in $Zr_{0.5}Hf_{0.5}NiSn$ based Heusler compounds for high power factors, *Applied Physics Letters* 2011, ***98***, 042106.

[20] S. Bhattacharya, V. Ponnambalam, A. Pope, P. Alboni, Y. Xia, T. Tritt, S. Poon, in *Thermoelectrics, 1999. Eighteenth International Conference on*, IEEE, **1999**, pp. 336.

[21] S. Bhattacharya, Y. Xia, V. Ponnambalam, S. Poon, N. Thadani, T. Tritt, in *MRS Proceedings, Vol. 691*, Cambridge Univ Press, **2001**, p. G7. 1.

[22] T. M. Tritt, S. Bhattacharya, Y. Xia, V. Ponnambalam, S. Poon, N. Thadhani, in *Thermoelectrics, 2001. Proceedings ICT 2001. XX International Conference on*, IEEE, **2001**, pp. 7.

[23] Y. F. Liu, P. Sahoo, J. P. A. Makongo, X. Y. Zhou, S. J. Kim, H. Chi, C. Uher, X. Q. Pan, P. F. P. Poudeu,Large Enhancements of Thermopower and Carrier Mobility in Quantum Dot Engineered Bulk Semiconductors, *Journal of the American Chemical Society* 2013, ***135***, 7486.

[24] J. P. A. Makongo, D. K. Misra, J. R. Salvador, N. J. Takas, G. Y. Wang, M. R. Shabetai, A. Pant, P. Paudel, C. Uher, K. L. Stokes, P. F. P. Poudeu,Thermal and electronic charge transport in bulk nanostructured $Zr_{0.25}Hf_{0.75}NiSn$ composites with full-Heusler inclusions, *Journal of Solid State Chemistry* 2011, ***184***, 2948.

[25] J. P. A. Makongo, D. K. Misra, X. Y. Zhou, A. Pant, M. R. Shabetai, X. L. Su, C. Uher, K. L. Stokes, P. F. P. Poudeu,Simultaneous Large Enhancements in Thermopower and Electrical Conductivity of Bulk Nanostructured Half-Heusler Alloys, *Journal of the American Chemical Society* 2011, ***133***, 18843.

[26] P. Sahoo, H. Djieutedjeu, P. F. Poudeu,Co_3O_4 nanostructures: the effect of synthesis conditions on particles size, magnetism and transport properties, *Journal of Materials Chemistry A* 2013, ***1***, 15022.

[27] N. J. Takas, P. Sahoo, D. Misra, H. F. Zhao, N. L. Henderson, K. Stokes, P. F. P. Poudeu,Effects of Ir Substitution and Processing Conditions on Thermoelectric Performance of p-Type $Zr_{0.5}Hf_{0.5}Co_{1-x}Ir_xSb_{0.99}Sn_{0.01}$ Half-Heusler Alloys, *Journal of Electronic Materials* 2011, ***40***, 662.

[28] C.-C. Hsu, Y.-N. Liu, H.-K. Ma,Effect of the $Zr_{0.5}Hf_{0.5}CoSb_{1-x}Sn_x$ / HfO 2 half-Heusler nanocomposites on the ZT value, *Journal of Alloys and Compounds* 2014, ***597***, 217.

[29] P. Sahoo, Y. F. Liu, J. P. A. Makongo, X. L. Su, S. J. Kim, N. Takas, H. Chi, C. Uher, X. Q. Pan, P. F. P. Poudeu,Enhancing thermopower and hole mobility in bulk p-type half-Heuslers using full-Heusler nanostructures, *Nanoscale* 2013, ***5***, 9419.

[30] Y. Liu, A. Page, P. Sahoo, H. Chi, C. Uher, P. F. Poudeu,Electronic and phonon transport in Sb-doped $Ti_{0.1}Zr_{0.9}Ni_{1+x}Sn_{0.975}Sb_{0.025}$ nanocomposites, *Dalton Transactions* 2014, ***43***, 8094.

[31] P. Sahoo, Y. Liu, P. F. Poudeu,Nanometer-scale interface engineering boosts the thermoelectric performance of n-type $Ti_{0.4}Hf_{0.6}Ni_{1+z}Sn_{0.975}Sb_{0.025}$ alloys, *Journal of Materials Chemistry A* 2014, ***2***, 9298.

[32] S. Chen, K. C. Lukas, W. Liu, C. P. Opeil, G. Chen, Z. Ren,Effect of Hf Concentration on Thermoelectric Properties of Nanostructured n-Type half-Heusler Materials $Hf_xZr_{1-x}NiSn_{0.99}Sb_{0.01}$, *Advanced Energy Materials* 2013, ***3***, 1210.

[33] G. Joshi, T. Dahal, S. Chen, H. Wang, J. Shiomi, G. Chen, Z. Ren,Enhancement of thermoelectric figure-of-merit at low temperatures by titanium substitution for hafnium in n-type half-Heuslers $Hf_{0.75-x}Ti_xZr_{0.25}NiSn_{0.99}Sb_{0.01}$, *Nano Energy* 2013, ***2***, 82.

[34] S. J. Poon, D. Wu, S. Zhu, W. Xie, T. M. Tritt, P. Thomas, R. Venkatasubramanian,Half-Heusler phases and nanocomposites as emerging high-ZT thermoelectric materials, *Journal of Materials Research* 2011, ***26***, 2795.

[35] S. Populoh, M. Aguirre, O. Brunko, K. Galazka, Y. Lu, A. Weidenkaff,High figure of merit in (Ti, Zr, Hf) NiSn half-Heusler alloys, *Scripta Materialia* 2012, ***66***, 1073.

[36] X. Yan, W. Liu, S. Chen, H. Wang, Q. Zhang, G. Chen, Z. Ren,Thermoelectric Property Study of Nanostructured p-Type Half-Heuslers (Hf, Zr, Ti) $CoSb_{0.8}Sn_{0.2}$, *Advanced Energy Materials* 2013, ***3***, 1195.

[37] X. Yan, W. Liu, H. Wang, S. Chen, J. Shiomi, K. Esfarjani, H. Wang, D. Wang, G. Chen, Z. Ren,Stronger phonon scattering by larger differences in atomic mass and size in p-type half-Heuslers $Hf_{1-x}Ti_xCoSb_{0.8}Sn_{0.2}$, *Energy & Environmental Science* 2012, ***5***, 7543.

[38] T. Kenjo, Y. Kimura, Y. Mishima, in *MRS Proceedings, Vol. 1218*, Cambridge Univ Press, **2009**, pp. 1218.

[39] J. Krez, J. Schmitt, G. J. Snyder, C. Felser, W. Hermes, M. Schwind,Optimization of the carrier concentration in phase-separated half-Heusler compounds, *Journal of Materials Chemistry A* 2014, ***2***, 13513.

[40] R. Downie, D. MacLaren, J.-W. Bos,Thermoelectric performance of multiphase XNiSn (X= Ti, Zr, Hf) half-Heusler alloys, *Journal of Materials Chemistry A* 2014, ***2***, 6107.

[41] M. Schwall, B. Balke,Phase separation as a key to a thermoelectric high efficiency, *Physical Chemistry Chemical Physics* 2013, ***15***, 1868.

Table of Contents Synopsis

Manipulating the band gap of ZrNiSn (half-Heusler) alloys through isoelectronic substitutions at Ti/Zr and Sn/Ge sites, and nanostructuring afford a simultaneous enhancement of thermopower and reduction in thermal conductivity leading to a significant increase in the *ZT* value.